Type Ia Supernovae forecast for the Zwicky Transient Facility Phase III

Andréa Antoniali
Supervised by Philippe Gris

May 31, 2023

Master Physique Fondamentale et Application
Univers et Particules

Contents

Acknowledgement

I want to thanks all the members of the cosmology group at the Laboratoire de Physique des Particles de Clermont-Ferrand, who welcomed me during my intership and provided a caring and joyful environment. I also want to thanks my supervisor Philippe Gris, who was the standardisable candle of my research during this internship, and managed to teach me how to do research in a new but exciting way, and was a moral and academic support during all this research venture. I also want to thanks Etienne Russeil for the discussions we have shared over a cup of tea, which always helped to make a breakthrough in my research. My thanks also goes to my parents, Valerie and Stéphane, who never cease to support me and help me the best they could, even if it meant listening to hazardous explanation about supernovae. Those thanks also goes to my brother Lucas, from which I had a constant supply of insights on my work, of jokes and words of encouragement, and never ceased to interest himself into my work. I thanks Raphaël Delhomme, from whom my initial spark of interest was sparked and nurtured, and who kept encouraging me into those studies. Finally, I want to thanks Jules Valroff-Marcelot and Theo Da Cunha for all the support they provided me during my studies this year, and for all the discussion into our respective fields of study.

1 Introduction

Einstein equation of general relativity links the geometry of the universe to its content. We want to measure the distance in the universe in a precise way to be able to constrain hypothesis and models on the content of the universe. To do so, we need cosmological probes, that is accurate means to measure distances in the cosmos. We will use Type Ia supernovae, transient astronomical events originating from the explosion of a white dwarf. We make the postulate that all those supernovae explode following the same physical process, and release each time the same amount of luminosity, making it possible to standardise them, and to measure their distance in the universe thanks to their apparent luminosity. With these distances measured, cosmological parameters are estimated from a Hubble Diagram.

In this Master's thesis, we'll lay a complete study from the cosmological basis to supernovae's theory aiming to use this knowledge to apply it to cosmological parameters calculations using the Fisher method. First, we lay the theoretical basis of our study : theoretical and observational cosmology, supernovae physics, and the statistical tools used. Then, we provide an analysis of our simulation and comparison between the Fisher method and the MINUIT algorithm usually used to fit a cosmological model. Finally, a basic forecast study related to the Zwicky Transient facility will be performed.

2 Cosmology

In this section, we will first explain the basis of theoretical cosmology such as the general theory of relativity, the metric used for our universe and how we describe its content. Then, we will present observational cosmology notion, such as the definition of the quantities used, and the Hubble diagram.

2.1 Theoretical cosmology

2.1.1 General relativity

The general relativity theory was developed during the early twentieth century. Albert Einstein wrote in 1905 three majors contribution to physics ; light quanta, Brownian motion and the premises of General Relativity as we know it, the theory of Special Relativity [Einstein(1905)]. Special relativity is a correction to Newton's laws for dynamics body : it makes correction for high velocity event and shows that an object has a relative time and length (space) depending of its relative velocity to the observer. Einstein decided to dig further and spent the next ten years trying to find an explanation to gravity and special relativity. He presented the Theory of General Relativity in 1915. With this theory, he opened a field of research and a new way to see physics and gravity, not as objects and forces, but as geometry itself. The keystone of General relativity is "Einstein Equivalence Principle", the local equivalence of gravitation and an inertial force (that is a force emerging from the fact of being in an accelerating frame of reference). Einstein managed to describe and understand special relativity as a manifestation of the space-time architecture : curvature and geometry are at the source of every gravitational forces. He postulates his principle as :

"At every space-time point in an arbitrary gravitational field it is possible to choose a locally inertial (or freely falling) coordinate system such that, within a sufficiently small region of this point, the laws of nature take the same form as in unaccelerated Cartesian coordinate systems in the absence of gravitation."[Weinberg & Steven(1972)]

k	Geometry	universe
+1	spherical	closed
-1	hyperbolic	open
0	euclidean	flat

Table 1: Different values of k and their meaning

Using this principle, a constant acceleration and a constant gravitational field cannot be distinguished locally. Einstein's general relativity can be expressed as :

Space and time are bent by their content in matter and energy.
Matter and energy are told how to move by the curved-space time [Ryden(2003)].

As shown in Einstein equations of fields [Blau(2023)] :

$$R_{\mu\nu} - \frac{1}{2}g_{\mu\nu}R + \Lambda g_{\mu\nu} = \frac{-8\pi G}{c^4}T_{\mu\nu} \tag{1}$$

where $T_{\mu\nu}$ is the energy-momentum tensor (in a empty space such as the void, $T_{\mu\nu} = 0$), $g_{\mu\nu}$ is the metric of our choice for space and time (as explained in section 2.1.2). $R_{\mu\nu}$ is the Ricci Tensor and R is a contraction of this Ricci tensor, known as the scalar curvature. Both are derived from the Riemann Tensor which describes the curvature of space and time given a specific metric [Blau(2023)]. Understanding the geometry of the universe and measuring distances in it informs us on its content. First, we'll discuss the geometry of the universe in section 2.1.2, then how to describe the content of the universe in terms of fluids in section 2.1.3 to finally expose the model used for describing its content in section 2.1.4.

2.1.2 The Friedmann–Lemaître–Robertson–Walker (FLRW) metric

To establish the geometry of the universe, we use general relativity. Einstein's equations of fields need a metric, describing how behaves space and time which are only one quantity here : space-time. A space-time metric must be invariant. The metric of space-time describing an euclidean space and a temporal space for the special relativity is Minkowski metric. This metric represents a euclidean flat space-time universe, with no curvature. In this metric, all the frames of reference[1] will agree on the total distance in space-time between events : $ds^2 = c^2dt^2 - dx^2 - dy^2 - dz^2 = \eta_{\mu\nu}dx^\mu dx^\nu$, with the metric of Minkoswki being represented as :

$$\eta_{\mu\nu} = \begin{pmatrix} 1 & 0 & 0 & 0 \\ 0 & -1 & 0 & 0 \\ 0 & 0 & -1 & 0 \\ 0 & 0 & 0 & -1 \end{pmatrix} \tag{2}$$

It works for special relativity problems, or Newtonian's physics (i.e not with speeds approaching the speed of light), but not for the scope of the whole universe where the objects are massive, the distance too large and measurements must account for the curvature of space-time. To describe an homogeneous and isotropic universe, we use the Friedmann–Lemaître–Robertson–Walker metric metric (also called FLRW) :

$$ds^2 = c^2dt^2 - a(t)^2\left(\frac{dr^2}{1-kr^2} + r^2(d\theta^2 + sin^2\theta d\phi^2)\right) \tag{3}$$

Where :

- a(t) is the dimensionless scale factor, used to characterise the expansion of the universe at a given time.
- r, θ, ϕ have the same roles as for spherical coordinates.
- k is the curvature and describes the geometry of the universe as shown in Table 1. For a flat universe, $k = 0$.

Using this metric, the first Friedman-Lemaître equation can be derived from Einstein equations (Eq 1) :

$$H^2 = (\frac{\dot{a}}{a})^2 = \frac{8\pi G}{3}\rho + \frac{\Lambda}{3} - \frac{k}{a^2} \tag{4}$$

where :

- $H = H(t)$ is the Hubble parameter dependent on time.

[1] All the different observers, no matter their velocity or their position.

- $H_0 = H(t_0)$ is the Hubble constant.
- $\rho = \rho(t)$ is the energy density of the universe content.
- Λ is the cosmological constant.

The crucial parameter is the Hubble parameter $H = \frac{\dot{a}}{a}$ which represent the rate of expansion of the universe. H_0 is the Hubble parameter corresponding to $t = t_0$, (t_0 being the time now) also known as the Hubble constant. The geometry provides us an equation to manipulate (Eq 4). We will present how to describe the matter of the universe in this equation.

2.1.3 Fluid equations

We describe the different parts of the Eq(4) as fluids with different energy densities ρ_i and pressure p_i and identified by their equation of state parameter w_i such as $p_i = w_i \rho_i$. The mass density to the scale factor relation is [Ryden(2003)][Rosnet(2023)]:

$$\rho(a) = \rho_0 \left(\frac{a}{a_0}\right)^{-3(w+1)} \tag{5}$$

with $\rho_0 = \rho(t_0)$, the mass density today. The parameters of state are for radiation $w_r = -\frac{1}{3}$, for matter $w_m = 0$ and for the cosmological constant density $w_\Lambda = -1$. Given this equation and those parameters, it can be shown that only the cosmological constant part can be responsible of the expansion of the Universe.

2.1.4 The ΛCDM model

Since the beginning of astronomy, several discoveries on the content of the universe have been made. In 1933, Zwicky observed that the redshift seen in the Coma cluster of nebulae indicates a density for the Coma system 400 greater that the one deduced from the observation of luminous matter[Zwicky(1933)], hence coming up with the idea of a dark matter, contributing but not visible by its light. This dark matter would allow us to the explain the rotational curves of galaxies. In 1968, Vera C. Rubin exposed that the rotation curves of stars and gas clouds inside the galaxies are more important at large radius than expected by know matter and the Newtonian laws. In 1998, the Hubble Diagram of made with type Ia Supernovae shows that not only the universe is expanding, but that it is also expanding at an accelerated rate [Perlmutter et al.(1999)Perlmutter, Aldering, & Goldhaber]. This dark energy fuelling this expansion makes for a huge majority of the energy content of the universe. Nowadays, it is estimated that dark energy is accounting for about 68.5% of the universe content, and the dark matter 31% of it, leaving only nearby 5% containing matter or energy known to us [et al.(2020)]. The model accounting for this expansion of the universe, describing it in three components (radiation, matter and the cosmological constant) is the Λ-Cold Dark Matter model, also known as the ΛCDM model. One can express the first equation of Friedmann-Lemaître, Eq(4) as :

$$\frac{8\pi G a^2}{3}(\rho_r + \rho_m + \rho_\Lambda - \rho_c) = k \tag{6}$$

with $H^2 = \frac{8\pi G \rho_c}{3}$, ρ_c being the critical mass density, and with the property of being the equal of the total densities of the others quantities if we are in an euclidean space : if $k = 0 \rightarrow \rho_c = \rho_r + \rho_m + \rho_\Lambda$.

We can rewrite the Friedman equation to get :

$$\frac{H^2}{H_0^2} = h^2(a) = \left[\Omega_{r,0}\left((\frac{a_0}{a}\right)^4 + \Omega_{m,0}\left(\frac{a_0}{a}\right)^3 + \Omega_{\Lambda,0} + \Omega_{k,0}\left(\frac{a_0}{a}\right)^2\right] \tag{7}$$

With $\rho_{c_0} = \frac{3H_0^2}{8\pi G}$ being the critical mass today.

$\mathbf{w_0 w_a}$CDM model : To try to better grasp the nature of dark energy, different models were proposed through the years, where the parameter w of the mass density of the dark energy is not a constant : $w_\Lambda = -1$,The value of w would be :

$$w(z) = w_0 + w_a(1-a) = w_0 + w_a \frac{z}{1+z} \tag{8}$$

This parametrisation allows us to consider an potential evolution of the parameter for the equation of state of the dark energy.

2.2 Observational Cosmology : Hubble diagram

2.2.1 Distance and measurements in cosmology

To understand our universe and its content, we need to be able to make measurement, hence the use of quantities such as the distance modulus μ, the redshift z and the luminosity distance D_L.
The cosmological redshift z can be derived from the Eq(3) :

$$1 + z = \frac{\dot{a_0}}{a(t)} = \frac{\lambda_0}{\lambda} \tag{9}$$

where a_0 is the expansion factor for the present time and a for a given time in the past. The observational redshift is directly linked to the scale factor and so to the Hubble parameter H.

For the rest of our study, we will assume that the universe is flat ($\Omega_{k,0} = 0$) and that the radiation density is negligible ($\Omega_{r,0} \approx 0$) :

$$h^2(z) = \Omega_{m,0}(1+z)^3 + \Omega_{\Lambda,0} \tag{10}$$

The luminosity distance is defined from the luminosity L of a source giving the flux [Ryden(2003)] :

$$F = \frac{L}{4\pi D_L^2} \tag{11}$$

where F is the flux received, L the distance between the observer and the source of the flux and D_L the luminosity distance.

$$D_L = (1+z)\frac{c}{H_0}\int_0^z \frac{dz'}{h(z, \Omega_m, \Omega_\Lambda), w} \tag{12}$$

The apparent magnitude m is the direct quantification of the light received from a light source by an observer. It is often used in comparison to another light source.

$$m_1 - m_2 = -2.5 \log_{10}\left(\frac{F_2}{F_1}\right) \tag{13}$$

The absolute magnitude M is the apparent magnitude of a star if it was at a distance of 10 parsecs[2] of the observer.

The distance modulus μ is the difference between the apparent magnitude m and the absolute magnitude M.

$$\mu = m - M = -2.5 \log_{10}\left(\frac{\frac{L}{4\pi D_L^2[pc]}}{\frac{L}{4\pi 10^2}}\right) = 5\log_{10}(D_{L[pc]}) - 5 = 5\log_{10}(D_{L[Mpc]}) + 25 \tag{14}$$

2.2.2 Hubble diagram

In 1929, Hubble published the Cepheid's Hubble Diagram 2. It was shown that galaxies farther away from us moved faster too as shown in Figure 2. He established a simple empirical law : $v = Hd$ where v is the velocity of the galaxies, H a linear coefficient to fit the data, and d the distance of those galaxies. Albeit a simple observation, it would lay ground to the next century of observational cosmology, as we're still aiming to draw Hubble Diagrams. The Hubble law is given at the first order by applying a Taylor series on the scale factor :

$$cz = H_0 d \tag{15}$$

Hubble diagrams can be used to understand the universe and its constituents, as explained in section 2.1.4. One example is show in Figure 3 where for higher redshifts, we see dissimilarities between our models. Thus, we'll need to have a way to look for high redshift events, allowing us to better constrain our cosmological parameters.

[2]One parsec (pc) is equal to 3.26 light-years.

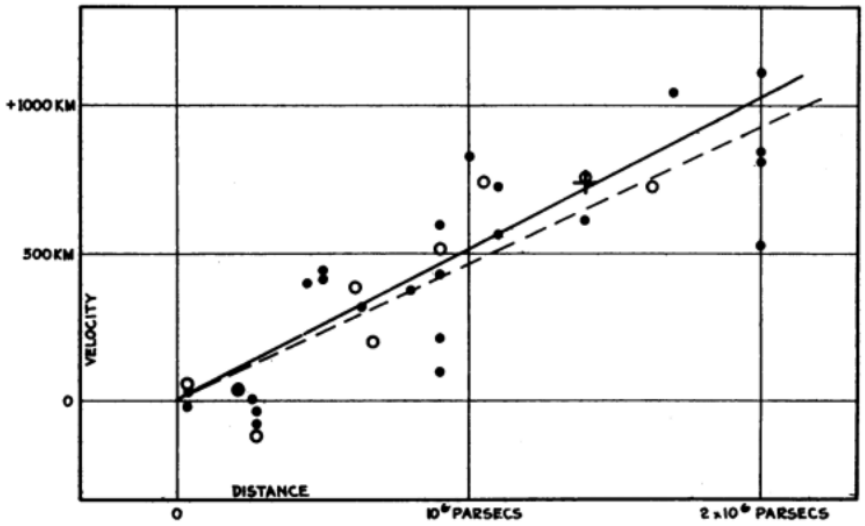

Figure 2: Original Hubble Diagram, representing the first observational evidence of the expansion of the universe. It shows the velocity on the distance relation for extra-galactic nebulae[Hubble(1929)].

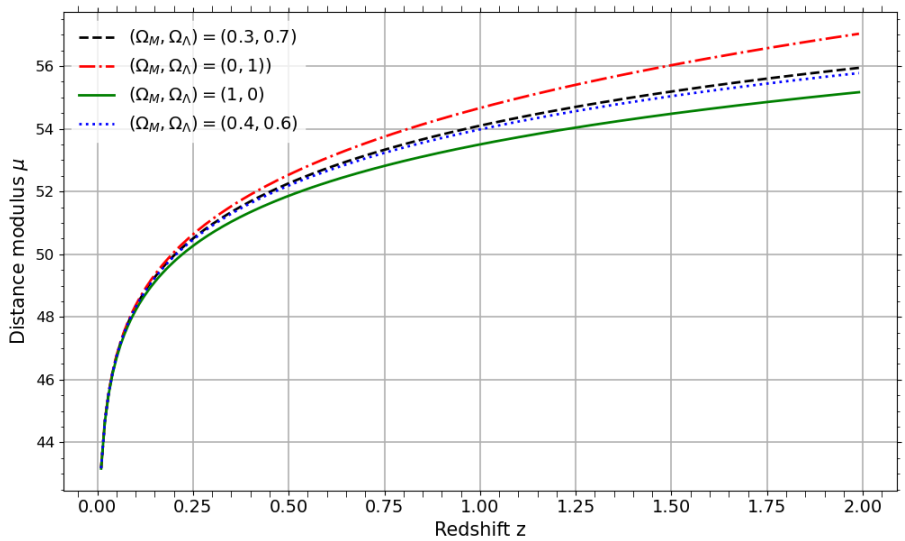

Figure 3: Hubble diagram with the distance modulus against the redshift for different cosmological parameters for the ΛCDM model.

3 Cosmological fit and Supernovae

This section presents the method to get measurement of the distance in the universe. First, the supernovae and their use as cosmological probe are presented, then the latest observations made with this method and finally how to standardise those supernovae for our model.

3.1 Supernovae

A supernova is a transient event, the explosion of a star emitting for a limited period of time a galaxy-like luminosity. Their luminosity is sometimes equivalent to the one of their host galaxy, allowing us to detect them from very far away. Type Ia supernovae are suppose to explode according to the same physical process allowing us to know their origin luminosity and deduce their distance. To understand how a supernovae arises, one need to understand the dynamics behind the evolution of the stars.

Evolution of stars into Supernovae

Stars are held together by two forces : the gravitational collapse of the star on itself, and the thermonuclear equilibrium of the fusion reaction inside its core, result of the pressure due to its mass. Depending on its mass, the star will burn more or less rapidly its fuel, the hydrogen composing it (the larger the star, the faster the process). This phase, in which the Sun currently is since approximately five billions years, is called the

main sequence. When a star has burned all of its hydrogen, the thermonuclear reaction keeping in check the gravitational collapse stops and a core collapse occurs. Depending on the mass, we have different scenarios :

- $M \leq 0.5 M_{\odot}$: Those star are red dwarf, and will burn their hydrogen for a very long time, much longer than the age of the universe (which is estimated to be 14 billions years).
- $0.5 M_{\odot} \leq M \leq 8 M_{\odot}$: Those stars will not be able to begin fusion of elements heavier than helium. When the helium will begin to be fused, the star will swell into a red giant, and when they will not have enough helium to maintain the outer pressure, it will contract itself into a white dwarf, the gravitational pressure being balanced by the electron degeneracy pressure. The outer layer becomes a planetary nebulae. Once the white dwarf is formed, it is possible that it gains enough mass to reach the Chandrasekhar's mass[3] [Mazzali et al.(2007)Mazzali, Ropke, Benetti, & Hillebrandt], which is the mass after which a star cannot be in equilibrium with the gravitational forces by sole electron-degeneracy pressure. As this mass reaches the Chandrasekhar's mass, its pressure and temperature gets higher, and finally it reignite a fusion process of its components provoking a Type Ia Supernova (SNIa). The process from which a white dwarf accretes more mass is subject to hypothesis and two scenarios are usually considered :
  - Single Degenerate model : In a binary system, the white dwarf gets its mass by accrediting via gravitation the matter of its paired star. As it gets more matter from its neighbouring star, the white dwarf can begin to do a fusion of its elements, exploding into a SNIa [Nomoto & Leung(2018)].
  - Double Degenerate Model : In this scenario, the two progenitors are both white dwarfs, and from an unknown process come to get closer from each other, fusing and provoking an SNIa [Liu et al.(2017)Liu, Wang, & Han].
- $M \geq 8 M_{\odot}$: They has enough mass to begin the fusion of heavier elements like carbon, oxygen or even silicium. They undergo the same steps as the stars with a lower mass, but will burn through more elements before collapsing. When the fusion reactions do not compensate the the gravitational crush, the star will collapse into either a black hole (if star's mass is more than 10 $M_{\odot}$ or a neutron star if it's less than that. Either way, the collapse occurs while ejecting the outer layers of the star, leading to a core collapse supernova.

3.1.1 Types of Supernovae

The Supernovae (SNe) are classified into historically into two mains classes [Minkowski(1941)] : Type I with hydrogen lines in their spectra, and Type II. The different types of SNe are shown in Figure 4.

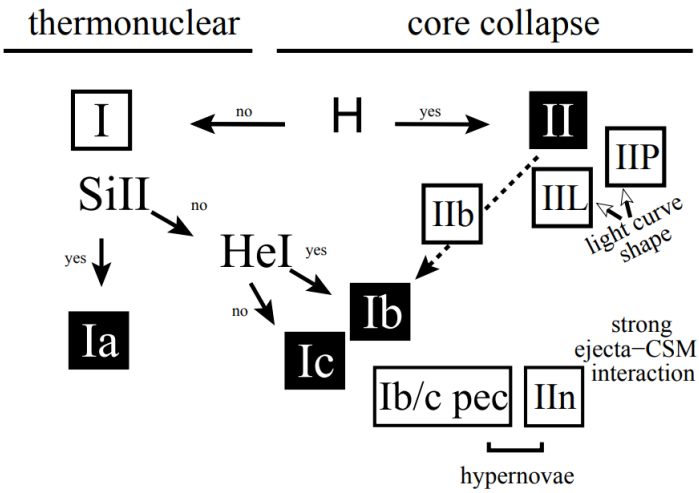

Figure 4: The current classification scheme of supernovae. Type Ia SNe are associated with the thermonuclear explosion of accreting white dwarfs. Other SN types are associated with the core collapse of massive stars. Some type Ib/c and IIn SNe with explosion energies $E > 1052$ erg are often called hypernovae [Turatto(2003)].

[3]For a white dwarf made of oxygen and carbon, it is estimated to be 1.44 $M_{\odot}$

3.1.2 SNe Ia

As seen in the Figure 4, only SNIa results from a thermonuclear explosion of a white dwarf. The mass limit inherent to the existence of white dwarf (they cannot have a mass superior to the Chandrasekhar mass or they have already collapsed under their own weight), indicates that they produce more homogeneous explosions, with almost the same starting mass (near 1.44 $M_{\odot}$). Resulting of this, the light curves and spectrum observed of SNIa are all relatively similar, allowing us to "standardise" them, and get an estimation of their distance. Type Ia supernovae are good candidates to probe the universe, and have been at the center of the efforts to get more accuracy on the cosmological parameters, along with other observational techniques such as the Baryon Acoustic oscillations, galaxy clusters surveys or weak lensing [Albrecht et al.(2006)Albrecht, Bernstein, & Cahn].

3.1.3 Hubble Fit

Cosmologists have collected more and more SNe Ia light curves to draw Hubble diagrams and constrain cosmological parameters. One of the last study was The Pantheon+ [Brout et al.(2022)Brout, Scolnic, & Popovic] in 2022, with over 1550 SNe Ia ranging from z = 0.001 to 2.26. The Hubble Diagram is shown in Figure 5.

Those diagrams are made with several parameters. Some are nuisance parameters to account of the various dissimilarities between SNe Ia (as explained in 3.2). The other parameters are the cosmological parameters we want to study. They are done by fitting the cosmological and nuisance parameters using a fitting method such as the Least Square Method (LSM).

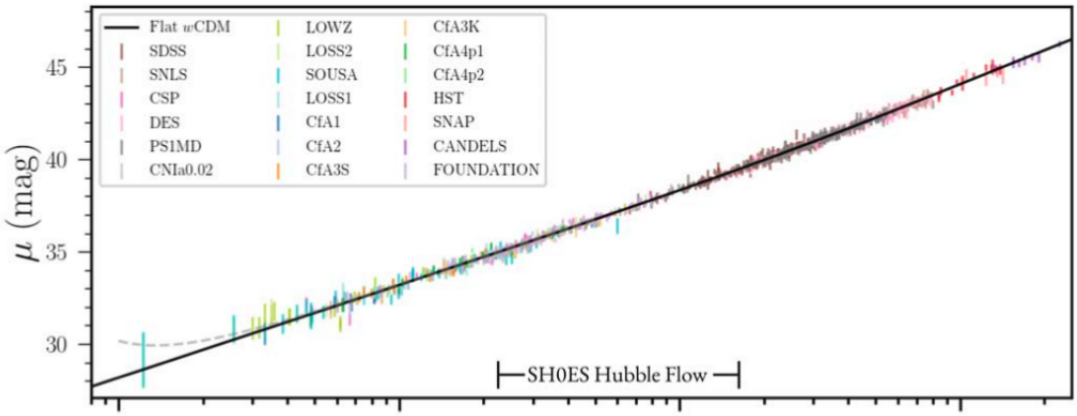

Figure 5: Top panel : Pantheon+ Hubble diagram of the distance modulus μ against the redshift z in the horizontal axis with different surveys, and the black line being the flat ΛCDM prediction. Bottom panel : Distance modulus residuals from the theory.

3.2 Standardisation of SNe Ia

We postulate that all SNe Ia explode with the same physical process, and since they have the same mass when the explosion occurs, they should have the same luminosity. Thus, we can use them as standardizable candle to measure their distance relatively to their redshift.

3.2.1 SALT2 : Light curve fit

SALT (Spectral Adaptative Light curve Template) is an empirical model of SNe Ia spectro-photometric evolution with time, trained on light-curves and spectra of observed SNe Ia. It provides a mean spectral sequence of SNe Ia and their variability parameters. The goal being to reduce the uncertainty on the measurement of the redshift observed, to be able to better constrain the cosmological parameters. We'll talk here about the widely used SALT[Guy, J. et al.(2007)Guy, J., Astier, P., & Baumont, S.].

SALT describes the density of flux F_{SN} received as :

$$F_{SN}(p,\lambda) = x_0[M_0(p,\lambda) + x_1 M_1(p,\lambda) + ...]e^{cCL(\lambda} \tag{16}$$

where p is the rest-frame time since the date of maximum luminosity in B-band : taking the time difference in days between the current observation t and the time of maximum luminosity t_0. The phase p is defined as $p = \frac{t_0 - t}{1+z}$, with z the redshift of the SN. λ is the wavelength in the rest-frame of the supernovae. M_i is the average spectral sequence for $k = 0$, whereas for $k > 0$, M_k describes the variability of the SNe Ia. Those parameters are properties of the global model.

In practice, we will use only this model to the first order, so with :

$$F_{SN}(p,\lambda) = x_0[M_0(p,\lambda) + x_1 M_1(p,\lambda)]e^{cCL(\lambda} \tag{17}$$

$Cl(\lambda)$ is the average color correction law. c is the color parameter describing the external sources of uncertainties such as the absorption by dust clouds of the host galaxies. It is expressed as : $c = (B-V)_{MAX} - \langle B-V \rangle$, with B and V the luminosity in band B and V. x_0 is the normalisation of the spectral energy distribution and x_1 is the stretch factor, that is equivalent in first approximation to Δm_{15} the difference in luminosity between the maximum of luminosity in the band B and 15 nights later. Those parameters are intrinsic of each SNe Ia.

3.3 Cosmological fit

3.3.1 Distance modulus

SALT is modelling SNe Ia light curves from which we can extract a distance modulus based on the principle that every SNIa has the same luminosity. One can express μ as :

$$\mu = m_b^* - M + \alpha x_1 - \beta c \tag{18}$$

where m_b^* the apparent magnitude in the B band, $x_1$and c are derived from the fit of the light curves. Those are the light curves parameters. M, the absolute magnitude, α and β are fitted by minimising the Hubble Diagram residuals and are the nuisance parameters.

3.3.2 χ^2 minimisation

We will minimise the χ^2 (Eq(18)) variable using the LSM. The χ^2 represents the deviation between our theoretical model predictions and the observations made during an experiment. It is found by maximising the log-likelihood function (more detailed in section 4.1.1) and assuming the measurement are independent and Gaussian variables [Cowan(1998)]:

$$\chi^2(\theta) = \sum_i \frac{(y_i - f(x_i,\theta))^2}{\sigma_i^2} \tag{19}$$

where y_i represent the observation, $f(x_i,\theta)$ the theoretical value expected given a function of x which depends on the unknown parameters $\theta = (\theta_1, \ldots, \theta_m)$, and σ_i is the uncertainty on the measurement. If the measurement are not independent, but still Gaussian, one can get this formula for the χ^2 value :

$$X^2(\theta) = \sum_{i,j=1}^{N} (y_i - f(x_i,\theta))(V^{-1})_{ij}(y_j - f(x_j,\theta)) \tag{20}$$

where V is the covariance matrix between the quantities measured. The more high quality observations made, the larger will be the χ^2 hence why use the ratio of χ^2 over the number of degrees of freedom
$ndf = n_{observations} - n_{parameters}$.

In cosmological models, the χ^2 has the form :

$$\chi^{\mathbf{2}} = \sum_{SN} \frac{(\mu_{exp} - \mu_{th})}{\sigma^2_{SN}} \tag{21}$$

where $\mu_{exp} = m_b^* - M + \alpha x_1 - \beta c$ and $\mu_{theo} = 5\log(D_{L[Mpc]}) + 25$.
Taking Eq (12) :

$$D_L = (1+z)\frac{c}{H_0}\int_0^z \frac{dz'}{h(z', \Omega_m, \Omega_\Lambda)}$$

The parameters to estimate are the cosmological parameters and the nuisance parameters. To get better estimations on a parameter uncertainty, we can constrain another parameter by adding a prior to the χ^2. This prior will change the χ^2 as if one parameter is well known, with a given uncertainty and measurement. Adding a prior is done as :

$$\chi^2_{prior(\theta_i)} = \chi^2 + prior = \chi^2 + \frac{(\theta_i - \theta_{ref,i})^2}{\sigma^2_{\theta_i}} \tag{22}$$

3.3.3 Figure of Merit (FoM)

To estimate if an experiment or a survey will be able to constrain the cosmological parameters, we may use a Figure of Merit(FoM). It has been used by the Dark Energy Task Force [Albrecht et al.(2006)Albrecht, Bernstein, & Cahn] to forecast the abilities of experiments to constrain cosmological parameters. It gives an indication on two parameters uncertainties much like the confidence ellipse. For a given area of a confidence ellipse [Coe(2009)], such as :

$$A = \pi\sigma_x\sigma_y\sqrt{1-\rho^2} \tag{23}$$

with $\rho = \frac{\sigma_{xy}}{\sigma_x\sigma_y}$ being the Pearson correlation coefficient, the FoM is defined as :

$$FoM = \frac{\pi}{A} = \frac{1}{\sigma_x\sigma_y\sqrt{1-(\frac{\sigma_{xy}}{\sigma_x\sigma_y})^2}} \tag{24}$$

In opposition to the area of the confidence ellipse that we want as small as possible, for the FoM, we aim for having the largest value. Thus, the more our FoM will grow, the more constraint will be the two parameters used to calculate it, giving an indication if our forecast is useful or not. The next part will be a study on how to get an estimation on the cosmological parameters and what strategy has been used to get the better FoM.

4 Estimation of cosmological parameters

The calculation of a full covariance matrix given a set of data can be computationally expensive : the matrix has to be inversed. Our systematical errors are correlated, which makes the matrix to be inverted not diagonal. It is a problem for large data sets such as the ones used in cosmology. This issue can be bypassed if the goal is to make using only the parameters errors to assess the survey. The Fisher information matrix will provide an estimate of the covariance matrix without having to estimate the parameters themselves, and being more efficient in computation time. We will use the Fisher information matrix to forecast the uncertainties on the parameters of the survey. First, the theory beneath the maximum likelihood fit method and Fisher will be presented. Then, we'll explain the creation of the module cosmo_fit.py that we will use for the rest of the analysis. Finally, we will present an analysis of the difference between the Fisher Method and the MINUIT method [Dembinski & et al.(2020)].

4.1 Theory

4.1.1 Maximum likelihood and fit

Considering a random variable x distributed according to a probability distribution function $f(x, \theta)$, with observations of this variable x, have an hypothesis for the function f and we do not know one of the parameters $\theta = (\theta_1, \ldots, \theta_m)$, we can establish a likelihood function as [Cowan(1998)]:

$$L(\theta) = \sum_{i=1}^{n} f(x_i, \theta) \tag{25}$$

This function is the likelihood according to the data points given the parameters given. Here, it is a like the probability distribution function (p.d.f) for x, but the only parameter is θ (x being already fixed by its observations.) Given that, one can find the estimator for the unknown parameter θ that maximises the likelihood function by finding the solution to the following function :

$$\frac{\partial L}{\partial \theta} = 0 \tag{26}$$

We have seen how to find the estimators of the parameters, the next step is to estimate the uncertainty of this estimates. We could try to compute analytically the variance, but in many cases it is too tedious or just impossible. One in those case uses the Rao-Cramer-Frechet (RCF) inequality, or information inequality, that gives a lower bound for an estimator's variance. This limit is given as [Cowan(1998)] :

$$V[\hat{\theta}] \geq \frac{\left(1 + \frac{\partial b}{\partial \theta}\right)^2}{E\left[\frac{\partial^2 \log(L)}{\partial^2 \theta^2}\right]} \tag{27}$$

where b is the bias of an estimator θ such as $b = E[\hat{\theta}] - \theta$ and L the likelihood function. An estimator is efficient in the case of an equality between the analytically found variance and the RCF inequality. If all our estimators are assumed efficient and with no bias, the inverse of the covariance matrix is :

$$(V^{-1})_{ij} = E\left[-\frac{\partial^2 log(L)}{\partial \theta_i \partial \theta_j}\right] \tag{28}$$

It is also called the Fisher information matrix. With sufficiently large data sample, the inverse of the variance bound given by RCF can be estimated by evaluating the second derivative of the expected value with the measured data and the maximum likelihood estimate $\hat{\theta}$:

$$\left(\hat{V^{-1}}\right)_{ij} = \left.\frac{-\partial^2 log(L)}{\partial \theta_i \partial \theta_j}\right|_{\theta=\hat{\theta}} \tag{29}$$

This is how is usually calculated the covariance matrix when the likelihood function is maximised numerically such as with MINUIT [Dembinski & et al.(2020)]. When MINUIT does its fit, it determines numerically the matrix of second derivative of the log-likelihood function using finite differences and then evaluate it at the maximum likelihood estimates for the parameters and invert it to find the covariance matrix [Cowan(1998)].

4.1.2 Fisher

The Fisher method will only give the lower bound of the RCF inequality, but no insigth on the parameters values. The interest in using the Fisher model is to predict how well an experiment will be able to constrain our model's parameters before we need to do it, doing the forecast of our experiment's potential results. A Fisher Matrix for two parameters (a, b) can be describe as : [Wittman(2023)]

$$[F] = \frac{1}{2}\begin{bmatrix} \frac{\partial^2}{\partial a^2} & \frac{\partial^2}{\partial a \partial b} \\ \frac{\partial^2}{\partial a \partial b} & \frac{\partial^2}{\partial b^2} \end{bmatrix} \chi^2 \tag{30}$$

With χ^2 being :

$$\chi^2 = \sum_i \frac{(y_i - f(x_i))^2}{\sigma_i^2} \tag{31}$$

where y_i represent the observation, $f(x_i)$ the theoretical value expected and σ_i is the uncertainty on the measurement.

So :

$$\frac{\partial \chi^2}{\partial x} = -2\sum_i \left(\frac{(y_i - f(x_i)}{\sigma_i^2}\right) f'(x_i)$$

$$\frac{\partial^2 \chi^2}{\partial x^2} = -2\sum_i \left(\frac{(y_i - f(x_i)}{\sigma_i^2}\right) f''(x_i) + 2\sum_i \frac{\partial f(x_i)}{\partial x}\frac{\partial f(x_i)}{\partial x}\frac{1}{\sigma_i^2}$$

$$\frac{\partial^2 \chi^2}{\partial x^2} \approx \frac{\chi^2(x_0 + \Delta x, y_0) - 2\chi^2(x_0, y_0) + \chi^2(x_0 - \Delta x, y_0)}{(\Delta x)^2} \tag{32}$$

$$\frac{\partial \chi^2}{\partial x} \approx \frac{\chi^2(x_0 + \Delta x, y_0) - \chi^2(x_0 - \Delta x, y_0)}{(2\Delta x)} \tag{33}$$

$$\frac{\partial^2 \chi^2}{\partial x \partial y} = \frac{\frac{\partial \chi^2}{\partial x}}{\partial y} \approx \frac{\partial}{\partial y}(\frac{\chi^2(x_0 + \Delta x, y_0)}{2\Delta x}) - \frac{\partial}{\partial y}(\frac{\chi^2(x_0 - \Delta x, y_0)}{2\Delta x}) \tag{34}$$

Using the Eq(33), we get :

$$\frac{\partial^2 \chi^2}{\partial x \partial y} = \frac{\chi^2(x_0 + \Delta x, y_0 + \Delta y) + \chi^2(x_0 - \Delta x, y_0 - \Delta y) - \chi^2(x_0 - \Delta x, y_0 + \Delta y) - \chi^2(x_0 + \Delta x, y_0 - \Delta y)}{4\Delta x \Delta y} \tag{35}$$

Using Eq(32) and Eq(35), we can now implement it numerically. For a linear function [Wittman(2023)] :

$$F_{ij} = \sum_b \frac{1}{\sigma_b^2}\frac{\partial f_b}{\partial p_i}\frac{\partial f_b}{\partial p_j} \tag{36}$$

Taking the example of $f(a, b)$:

$$F^{-1} = \begin{bmatrix} \sigma_a^2 & \sigma_{ab} \\ \sigma_{ab} & \sigma_b^2 \end{bmatrix} = V \tag{37}$$

4.2 Numerical implementation

We developed a python module called cosmo_fit.py[4] able to :

- Allow the user to define a χ^2 function to minimise and the function defining the model. For this, an abstract class is used, where the user program inherit of the class cosmoFit and has to manually insert their model, parameters and way of calculating the χ^2 value.
- Take as an entry an hdf5 [The HDF Group(2000-2010)] file composed of a number of samples tables, each containing three entries : "z" : the redshift completeness, "mu" the distance modulus used to generate the redshift completeness and "sigma", an uncertainty linearly extrapolated between 0.001 and 0.06 and applied on the redshift generated. As meta data of this hdf5 file, we have the cosmological parameters used to generate the data.
- Add priors on parameters.

[4] `https://github.com/LSSTDESC/sn_phystools/tree/dev/sn_cosmology`

- returns the numerical analysis in a panda dataframe [pandas development team(2020)].
- Add constraints on our parameters of fit.

The goal of this numerical implementation is to validate the Fisher approach versus the fit approach and to use the Fisher approach to do a forecast for given data on selected parameters. A comparative study will be done in section 4.3.

4.2.1 Toy model : Perret's rate distribution

To create different cosmology models, with different parameters of fit, we want a distribution of SNe Ia distance modulus by redshift. The Perrett's rate[Perrett et al.(2012)Perrett, Sullivan, & Conley] will be use. This rate states that for a redshift z included in $0.1 < z < 1.1$, the rate of supernovae is :

$$r = (1+z)^{\alpha} \tag{38}$$

where $\alpha = 2.11 \pm 0.28$
Using this rate, a number of SNe Ia was generated in the range $z \in [0.1, 1.1]$ according to a random law based on Eq(38), as shown in Figure 12.

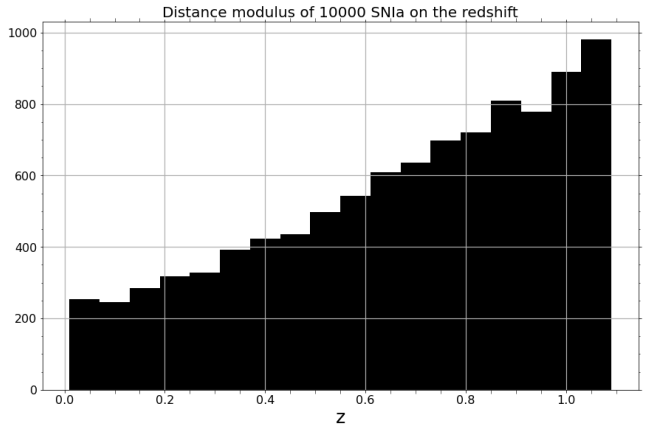

Figure 6: Histogram of the distribution of the redshift position of the SNe Ia that will be used for the test in the section 4.3.

4.3 Results

We present the uncertainties and the statistics between the Fisher method and the MINUIT method, Different configuration are shown at each step : Configuration 1 with no prior, and Configuration 2 with a prior on Ω_m added to the χ^2 value, as explained in 3.3.2. These configuration are shown in Table 2. First will be discussed the results for the parameters $w0$ and w_a, then the Ω_m parameter and finally the time of computation and the FoM.

	Parameters	Prior
Configuration 1	Ω_m, w_0, w_a	$\Omega_m = 0.3 \pm 0.0073$
Configuration 2	Ω_m, w_0, w_a	-

Table 2: Configurations of our cosmology and fit

The uncertainty displayed in the relative difference, the fisher parameter being a and MINUIT b, is calculated as the uncertainty of the function $f(a,b) = \frac{a-b}{b}$:

$$\sigma_{f(a,b)} = \left(\frac{\partial f}{\partial a}\right)^2 \sigma_a^2 + \left(\frac{\partial f}{\partial b}\right)^2 \sigma_b^2 + 2\frac{\partial f}{\partial a}\frac{\partial f}{\partial b}\sigma_{ab} \tag{39}$$

$$\sigma_{ab} = r_{ab}\sigma_a\sigma_b \tag{40}$$

r_{ab} being the sample correlation coefficient between two variable a and b :

$$r_{ab} = \frac{\sum_i [(a_i - \bar{a})(b_i - \bar{b})]}{\sqrt{\sum_i (a_i - \bar{a})^2 * \sum_i (b_i - \bar{b})^2}} \tag{41}$$

Then,

$$\sigma_{f(a,b)} = \left(\frac{\partial f}{\partial a}\right)^2 \sigma_a^2 + \left(\frac{\partial f}{\partial b}\right)^2 \sigma_b^2 + 2\frac{\partial f}{\partial a}\frac{\partial f}{\partial b}\sigma_a\sigma_b r_{ab} \tag{42}$$

Finally having for the uncertainty:

$$\sigma_{f(a,b)} = \frac{1}{b^2}\sigma_a^2 + \frac{a^2}{b^4}\sigma_b^2 - 2\frac{a}{b^3}\sigma_a\sigma_b r_{ab} \tag{43}$$

4.3.1 Uncertainty on w_0

Figure 7 shows the evolution of the uncertainty σ_{w0} with the number of SNe Ia.

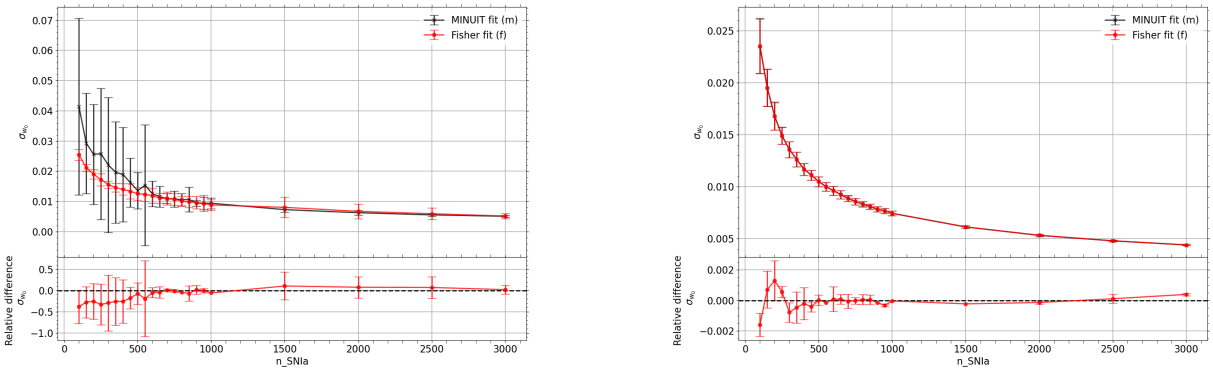

(a) Configuration 1

(b) Configuration 2

Figure 7: Uncertainty of σ_{w0} on the number of SNIa. The data are the means of 100 samples and the error is the standard deviation observed. The bottom graphs are the relative difference between the MINUIT and Fisher results such as : $\Delta\sigma_{w0} = \frac{fisher-minuit}{minuit}$.

With no prior (Figure 7a), the difference between Fisher and MINUIT is that Fisher overestimates the precision of the measurement of w_0 and seems to be less subject to fluctuation as MINUIT. With no prior, it is seen that $\frac{\sigma_{w_0}}{w_0} < 1\%$ for $n > 1000$, The relative difference is under 10 % for a number of SNe Ia superior to 600. With a prior (Figure 7b), the difference between MINUIT and Fisher is less than 0.01 %. With the prior, it is seen that $\sigma_{w_0} < 1\%$ for $n > 600$, where n is the number of SNe Ia taken for the fit.

4.3.2 Uncertainty on w_a

Figure 8 shows the evolution of the uncertainty of σ_{wa} with the number of SNe Ia.

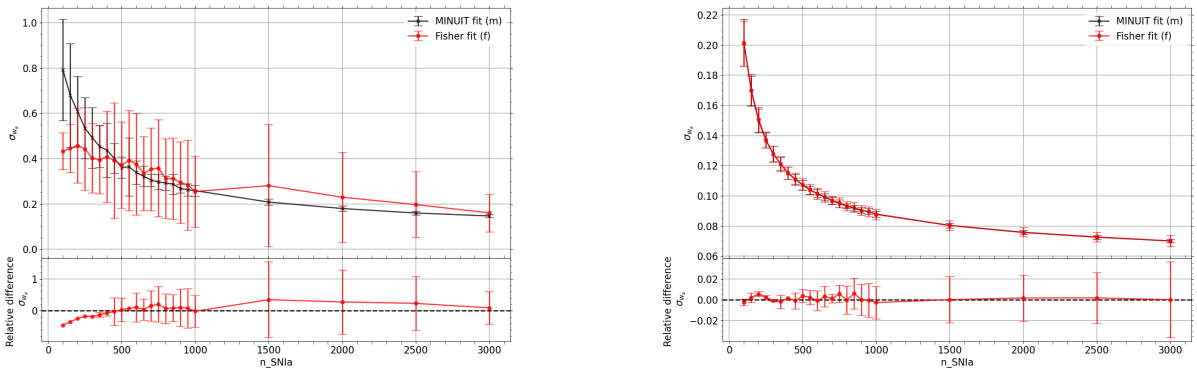

(a) Configuration 1

(b) Configuration 2

Figure 8: Uncertainty of σ_{wa} on the number of SNIa. The data are the means of 100 samples and the error is the standard deviation observed. The bottom graphs are the relative difference between the MINUIT and Fisher results such as : $\Delta\sigma_{wa} = \frac{fisher-minuit}{minuit}$.

With no prior (Figure 8a), Fisher has a higher fluctuation of its uncertainty on w_a than MINUIT but the results seems to be converging for higher numbers of SNe Ia with a relative uncertainty between Fisher and MINUIT of 23% for $n(SNeIa) > 2500$. With higher numbers, both methods lead to some results, the Fisher uncertainty fluctuations being higher than the w_a's one. With a prior (Figure 8b), the difference between MINUIT and Fisher is under 0.5%, but the fluctuation grows with the number of SNIa. With a prior, there is $\sigma(w_a) < 7\%$ asymptotically ($n > 3000$)

4.3.3 Uncertainty on Ω_m

Figure 9 shows the evolution of σ_{Ω_m} with the number of SNe Ia.

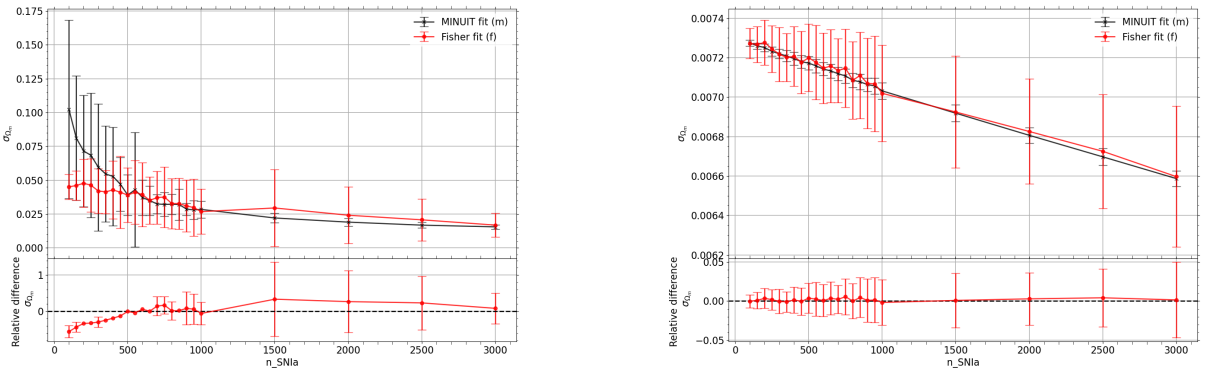

(a) Configuration 1

(b) Configuration 2

Figure 9: Uncertainty of σ_{Ω_m} on the number of SNIa. The data are the means of 100 samples and the error is the standard deviation observed. The bottom graphs are the relative difference between the MINUIT and Fisher results such as : $\Delta\sigma_{\Omega_m} = \frac{fisher-minuit}{minuit}$.

With no prior (Figure 9a), we see an overestimation of the accuracy of the measurement by the Fisher method, but still with within the uncertainty of the MINUIT fit. There is$\sigma_{\Omega_m} < 1\%$ for $n > 2500$, where n is the number of SNe Ia taken for the fit. With a prior (Figure 9b), the fluctuation of σ_{Ω_m}, the relative difference between Fisher and MINUIT is under 0.5%, which can be explained by the constraint put by the prior on the parameter Ω_m.

4.3.4 Time of processing

The Figure 10 shows the evolution of the time of execution of one fit (be it by Fisher or MINUIT) with the number of SNe Ia. This comparison is important : it will determine the interest of using Fisher and not MINUIT for the forecast.

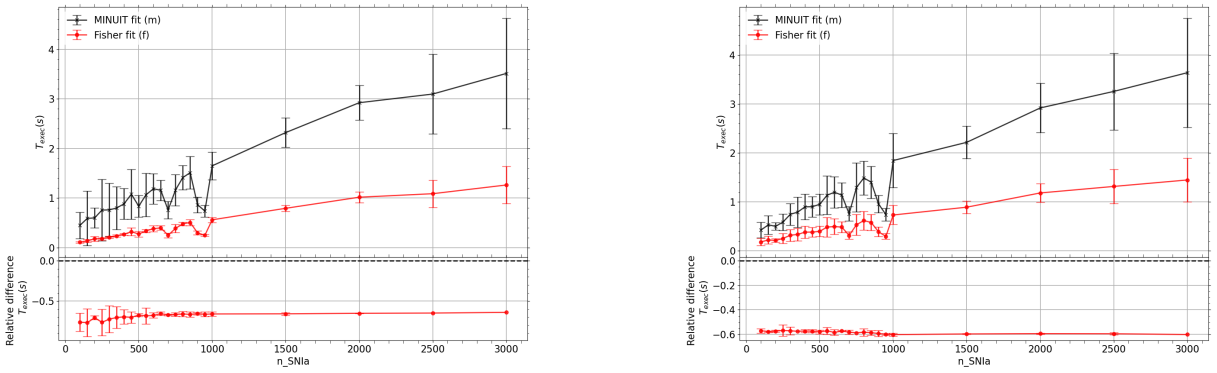

(a) Configuration 1

(b) Configuration 2

Figure 10: Uncertainty of the time of execution on the number of SNIa. The data are the means of 100 samples and the error is the standard deviation observed. The bottom graphs are the relative difference between the MINUIT and Fisher results such as : $\Delta T_{exec} = \frac{fisher-minuit}{minuit}$.

We see in the Figure 10 that the MINUIT results are all above for the time of calculation in comparison to the Fisher time.

We have a gain of time of the Fisher method on the MINUIT method of a factor 3 in average.

4.3.5 Figure of Merit

We use the FoM, as seen in section 3.3.3, to have an estimation of our overall accuracy on two parameters at once : w_a and w_0 as shown in Figure 11.

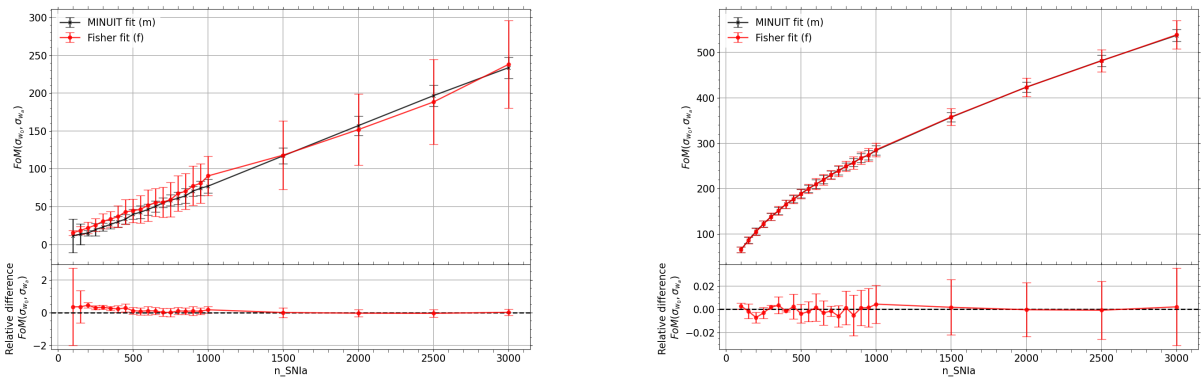

(a) Configuration 1

(b) Configuration 2

Figure 11: FoM as a function of the number of SNIa. The data are the means of 100 samples and the error is the standard deviation observed. The bottom graphs are the relative difference between the MINUIT and fisher results such as : $\Delta FoM = \frac{fisher - minuit}{minuit}$.

We can see on Figure 11a, that the higher the FoM, the more constrained our parameters are. For more than 1500 SNIa, the relative difference between Fisher and MINUIT is less than 5%. On Figure 11b, where a prior has been added to the χ^2, the difference between Fisher and MINUIT is under 0.025 %, and yet, the standard deviation of the relative measurement is higher. The augmentation of the fluctuation of the Fisher uncertainty needs to be addressed in future study. We can say that overall Fisher is similar to the MINUIT method in its results for the FoM to replace it.

4.3.6 Cross-check of the pull on w_0

We will check if our implementation is robust. For that, we can estimate the pull on the the parameter w_0 and check if its distribution follows a normal law.

We see that the distribution of prediction for w_0 follows a normal distribution law, which is a check of its robustness.

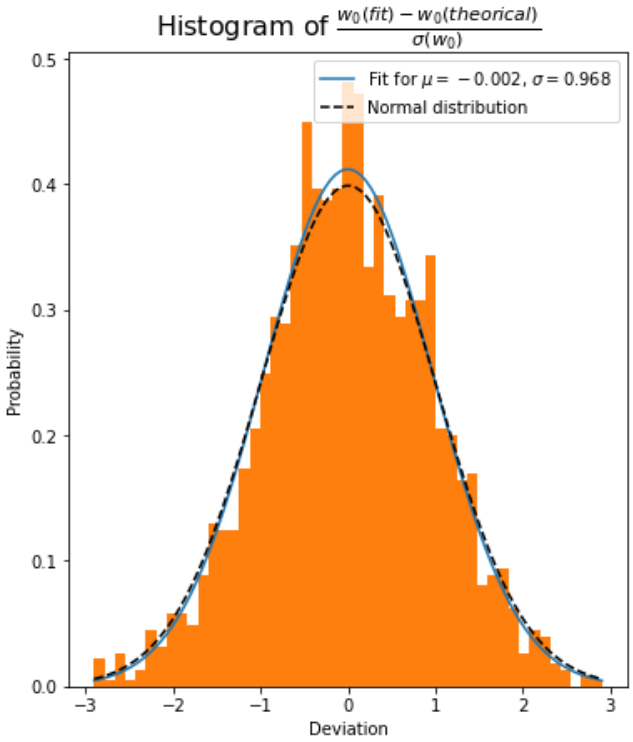

Figure 12: Histogram of the pull on the parameter w_0, with a prior.

5 Cosmology forecast with the Zwicky Transient Facility

As seen in the last section, the Fisher method can be used to forecast results in place of the LSM, with a gain of time. This section will discuss how to forecast a survey with different observations parameters. First, the technical aspect of the Zwicky Transient Facility will be presented, then the limitations and finally the observing simulation strategy with the results.

5.1 Technical aspects

The Zwicky transient Facility is installed on the 122 centimetres Samuel Oscin Telescope located on the Mount Palomar in California, at the United States of America. It aims to detect transient events ; which are astronomical phenomenon that are changing in luminosity over a relatively short period of time, such as asteroids and supernovae.
It specificity are [Dekany et al.(2020)Dekany, Smith, & Riddle]:

- 16 CCD for a total of 600 megapixel.
- a field of view of 47 square-degree, each image covering 235 times the area of the full moon.
- an exposure time of 30 seconds, and a
- three filters : green, red, infrared.

ZTF is able to cover the whole northern hemisphere sky in only 2 nights of observation by focusing on having a large field of view (as shown in Figure 13).

5.2 Limitations : Redshift completeness

The survey is limited by several factors into the number of SNe Ia that can be detected, some are linked to the condition of the experiment, such as the Malmquist effect or even purely physical phenomenon, such as the dust found in the Milky Way.

5.2.1 Malmquist bias

The Malmquist bias is an effect that occurs in observational astronomy with limited flux observation (so limited in time), where the low luminosity object are less accounted for than the brighter, no matter their distance. For

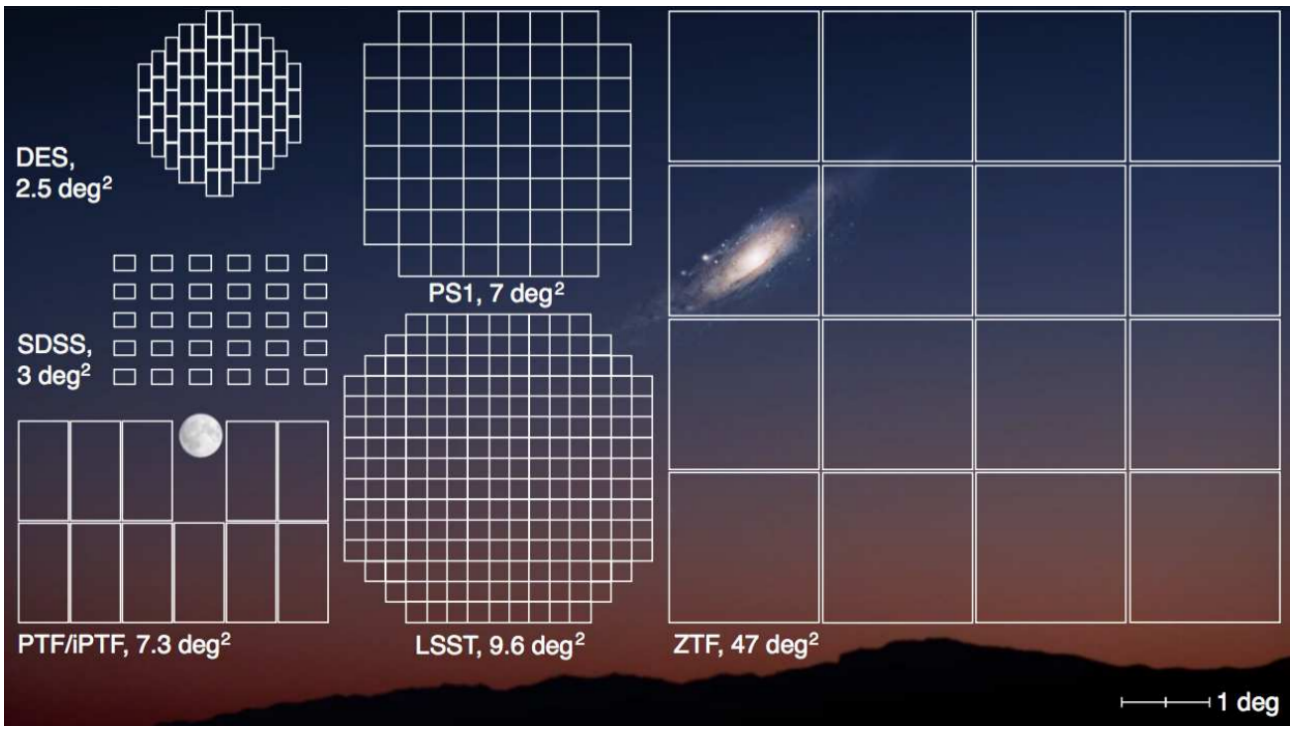

Figure 13: Zwicky Transient Facility camera field of view compared to other cameras such as LSST. The Moon and the Andromeda Galaxy (Messier 31) are shown to scale. [Laher et al.(2017)Laher, Masci, & Groom]

a given field of the sky, as the distance to rises, the more luminous events are more taken into account than the less luminous one. It leads to an over-representation of those more luminous object and can affect measurement of mean magnitude on a given portion of the sky. In summary, the Malmquist bias prohibits the survey to see the less luminous supernovae at higher redshift. Since it is affecting the measurement of the magnitude, it is also influencing the measurement of the distance modulus and is a source of systematic uncertainty on our measurement.It can be corrected [Teerikorpi(2015)], but must still be accounted for in our uncertainties calculation.

5.2.2 Redshift completeness

The Malmquist bias is affecting our observations of SNe Ia by lowering the amount of low luminosity SNe Ia at higher redshift: SNe Ia are lost as the redshift goes higher. A limit is established, called the redshift completeness, below which no SNe Ia are lost due to their luminosity. The higher this redshift completeness is, the more SNe Ia will be observed and the more constrained the cosmological parameters will be. Moreover, to detect tenuous deviation from actual data, high redshift SNe Ia are needed, since the deviation from the cosmological parameter is more present for higher redshift as seen in in Figure 3.

5.3 Observing strategy

The observing strategy (i.e the experimental configuration : numbers of visits, cadence, condition of observation, and budget of time allowed) will affect the physic studied and the data collected. For example, since the time of observation per night is limited, a choice must be made between the band observed and their time of exposure. More than that, astronomical surveys are also subject to atmospheric perturbations, such as clouds or even the brightness of the moon, and as such it can affect the observations and the period exposition. The simulations used for the forecast will first be explained, then the parameter used to access the redshift completeness and finally the results will be presented.

5.3.1 ztf_simpipe

ztf_simpipe[5] is a pipeline used to simulate data from ZTF with different observing strategies. The users writes the observing configuration in a csv file and after lunching a script, it will process the simulations. First, FakeObs.py, a python script, will generate fake observations given the configuration written in the configuration csv file. Then, a python script called prod_sn.py will take the fake observations given by FakeObs.py, simulate

[5] https://github.com/pgris/ztf_simpipe

their light curves, apply a selection (that can be tuned by the user), fit the light curves and give back a hdf5 file containing all the information of fit and on the cosmology in a range of redshift $[z_min, z_max]$. These light curves are then used to deduce the redshift completeness. At the end of this pipeline, the information provided are :

- an hdf5 file with faint supernovae generated ($x_1 = -2.0$, $c = 0.2$).
- an hdf5 file with the light curves of those SNIa and the one selected given fixed conditions.
- an hdf5 file fiiting those light curves to get standardised SNe Ia, with the parameters of fit.

Once these SNe Ia generated, they are merged into a single panda dataframe containing all the range of redshift $[z_min, z_max]$.

The observing parameters that are played upon are written in a csv file, and the program can select into this csv file the configuration needed. These parameters are the cadence of observation in the band g, r, and i and the number of observation per pixel. The cadence of observation is the number of night between two observation for a portion of the sky for a particular band, and the number of observation in a band. Once the simulations are done, the redshift completeness depending on the observing configuration must be calculated.

5.3.2 Redshift completeness z_{lim}

The redshift completeness limit depends on a lot of parameters, and the time lacked for a through analysis of each small deviations of it. It can be found that for high redshift values, [Gris et al.(2023)Gris, Regnault, & Awan], the uncertainty of the colour fit parameter σ_c is a good indication of our redshift completeness limit :

$$\sigma_c \leq 0.04 \rightarrow z_{lim} \tag{44}$$

The strategy to determine z_{lim} will be to interpolate the values of σ_c for their redshift, and to select the redshift at $\sigma_c = 0.04$.

5.3.3 Results

With the data generated by the pipeline, we can estimate the value of z_{lim} as shown in Fig 14.

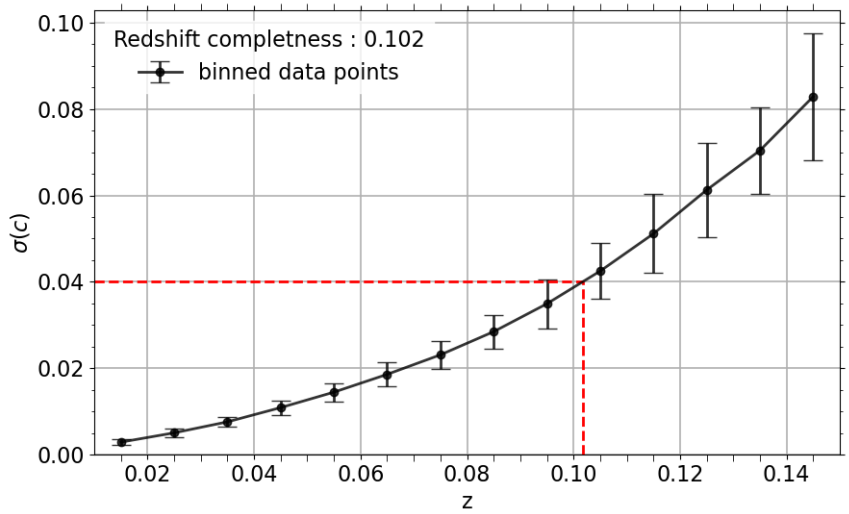

Figure 14: σ_c as a function of the redshift for the configuration 1 (see Table 3). The dashed red line represents the value of z_{lim} for a $\sigma_c = 0.04$.

σ_c increases with the z, as the signal-to-noise ration of the light curves decreases with the z. In Fig 14, $\sigma_c = 0.04 \rightarrow z_{lim} = 0.102$.

A list of all the configurations generated can be found in the Table 3). The next step will be to do this interpolation for different configuration, and compare them based on the z_{lim} obtained, as shown in Figure 15. One can see that the best redshift is for the Configuration 9. A look at the Table 3 gives its characteristics : a cadence of one night for g and r band, a cadence of two for the i band, and a observation for each band. Looking at the four higher redshift configuration (Table 4), one see that while the g band is important, having observations in every band is essential, and that the i band is crucial to see observer higher z events.

config	cad_g	cad_r	cad_i	N_g	N_r	N_i
conf1	2	2	4	1	1	1
conf2	2	2	4	1	1	0
conf3	2	2	4	1	0	1
conf4	2	2	4	0	1	1
conf5	2	2	4	2	1	0
conf6	2	2	4	1	2	0
conf7	2	2	4	0	1	2
conf8	2	2	4	0	2	1
conf9	1	1	2	1	1	1
conf10	1	1	2	1	1	0
conf11	1	1	2	1	0	1
conf12	1	1	2	0	1	1
conf13	1	1	2	2	1	0
conf14	1	1	2	1	2	0
conf15	1	1	2	0	1	2
conf16	1	1	2	0	2	1
conf17	4	2	2	1	1	1
conf18	4	2	2	1	1	0
conf19	4	2	2	1	0	1
conf20	4	2	2	0	1	1
conf21	4	2	2	2	1	0
conf22	4	2	2	1	2	0
conf23	4	2	2	0	1	2
conf24	4	2	2	0	2	1

Table 3: Different configuration of observations : "cad" means the cadence (i.e the number of night between each visit, "N" is the number of observations during a visit.

config	cad_g	cad_r	cad_i	N_g	N_r	N_i
conf9	1	1	2	1	1	1
conf10	1	1	2	1	1	0
conf13	1	1	2	2	1	0
conf14	1	1	2	1	2	0

Table 4: Best configurations of observation based on Figure 15

6 Conclusion

After introducing the basis of cosmology, and the use of type Ia supernovae for constraining the cosmological parameters, a study of the interest of the Fisher method against MINUIT has been performed. As per the literature [Wittman(2023)] described, a gain of computational cost was made in the expanse of little accuracy. Afterwards, a preliminary survey with ZTF was studied, revealing the importance of using the band i to go to higher redshift. A further development would be to refine the analysis on the redshift completeness, by taking more parameters into account, and to use the Fisher method to perform quicker calculations. Pursuing the study on the ZTF survey would mean simulating all types of SNe Ia, increase the number of visits per night and estimate the cosmological impact by drawing a Hubble diagram with those simulated SNe Ia using the Fisher approach developed in this study.

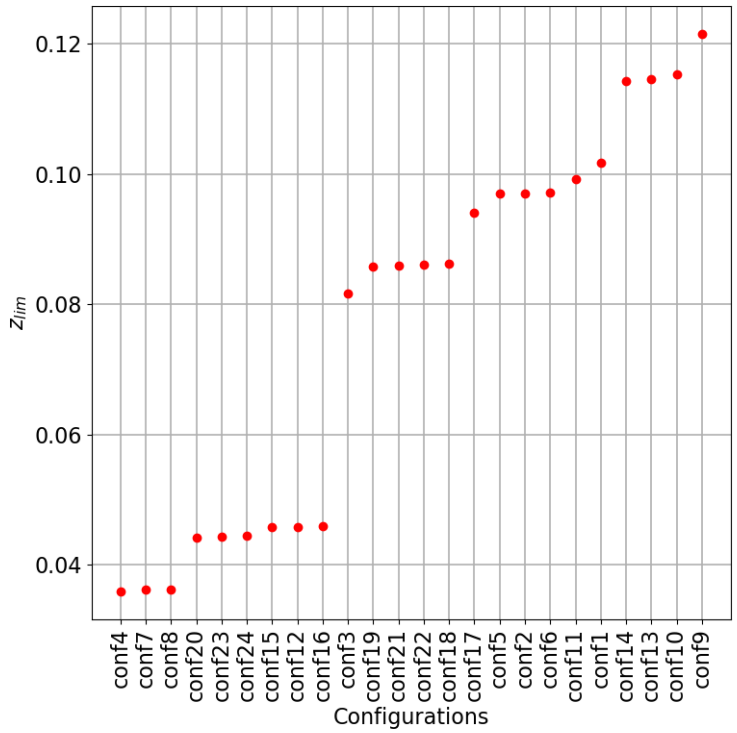

Figure 15: Redshift completeness limit for different configurations (see Table 3).

References

[Albrecht et al.(2006)Albrecht, Bernstein, & Cahn] Albrecht, A., Bernstein, G., & Cahn, R. 2006, Report of the Dark Energy Task Force

[Blau(2023)] Blau, M. 2023, Lectures Notes on General Relativity

[Brout et al.(2022)Brout, Scolnic, & Popovic] Brout, D., Scolnic, D., & Popovic, B. 2022, The Astrophysical Journal, 938, 110

[Coe(2009)] Coe, D. 2009, Fisher Matrices and Confidence Ellipses: A Quick-Start Guide and Software

[Cowan(1998)] Cowan, G. 1998, Statistical data analysis (Oxford University Press, USA)

[Dekany et al.(2020)Dekany, Smith, & Riddle] Dekany, R., Smith, R. M., & Riddle, R. 2020, Publications of the Astronomical Society of the Pacific, 132, 038001

[Dembinski & et al.(2020)] Dembinski, H. & et al., P. O. 2020

[Einstein(1905)] Einstein, A. 1905, Annalen Phys., 17, 891

[et al.(2020)] et al., P. 2020, A&A, 641, A6

[Gris et al.(2023)Gris, Regnault, & Awan] Gris, P., Regnault, N., & Awan, H. 2023, The Astrophysical Journal Supplement Series, 264, 22

[Guy, J. et al.(2007)Guy, J., Astier, P., & Baumont, S.] Guy, J., Astier, P., & Baumont, S. 2007, A&A, 466, 11

[Hubble(1929)] Hubble, E. 1929, Proceedings of the National Academy of Sciences, 15, 168

[Laher et al.(2017)Laher, Masci, & Groom] Laher, R. R., Masci, F. J., & Groom, S. 2017, Processing Images from the Zwicky Transient Facility

[Liu et al.(2017)Liu, Wang, & Han] Liu, D., Wang, B., & Han, Z. 2017, Monthly Notices of the Royal Astronomical Society, 473, 5352

[Mazzali et al.(2007)Mazzali, Ropke, Benetti, & Hillebrandt] Mazzali, P. A., Ropke, F. K., Benetti, S., & Hillebrandt, W. 2007, Science, 315, 825

[Minkowski(1941)] Minkowski, R. 1941, , 53, 224

[Nomoto & Leung(2018)] Nomoto, K. & Leung, S.-C. 2018, Space Science Reviews, 214

[pandas development team(2020)] pandas development team, T. 2020, pandas-dev/pandas: Pandas

[Perlmutter et al.(1999)Perlmutter, Aldering, & Goldhaber] Perlmutter, S., Aldering, G., & Goldhaber, G. 1999, The Astrophysical Journal, 517, 565

[Perrett et al.(2012)Perrett, Sullivan, & Conley] Perrett, K., Sullivan, M., & Conley, A. 2012, The Astronomical Journal, 144, 59

[Rosnet(2023)] Rosnet, P. 2023, Lectures Notes on Cosmology

[Ryden(2003)] Ryden, B. 2003, Introduction to cosmology

[Teerikorpi(2015)] Teerikorpi, P. 2015, Astronomy &amp Astrophysics, 576, A75

[The HDF Group(2000-2010)] The HDF Group. 2000-2010, Hierarchical data format version 5

[Turatto(2003)] Turatto, M. 2003, in Supernovae and Gamma-Ray Bursters (Springer Berlin Heidelberg), 21–36

[Weinberg & Steven(1972)] Weinberg, S. & Steven, W. 1972, Gravitation and Cosmology: Principles and Applications of the General Theory of Relativity (Wiley)

[Wittman(2023)] Wittman, D. 2023, Fisher Matrix for Beginners

[Zwicky(1933)] Zwicky, F. 1933, Helvetica Physica Acta, 6, 110